2010 IEEE International Conference on Robotics and Automation
Anchorage Convention District
May 3-8, 2010, Anchorage, Alaska, USA

A Variable Physical Damping Actuator (VPDA) for Compliant Robotic Joints

Matteo Laffranchi[1,2], Nikos G. Tsagarakis[1], and Darwin G.Caldwell[1]

[1]Italian Institute of Technology (IIT), Genova 16163, Italy

[2]The University of Sheffield, Western Bank Sheffield, S10 2TN, UK

Abstract— **This paper introduces the development of a semi-active friction based variable physical damping actuator (VPDA) unit. The realization of this unit aims to facilitate the control of compliant robotic joints by providing physical variable damping on demand assisting on the regulation of the oscillations induced by the introduction of compliance. The mechatronics details and the dynamic model of the damper are introduced. The proposed variable damper mechanism is evaluated on a simple 1-DOF compliant joint linked to the ground through a torsion spring. This flexible connection emulates a compliant joint, generating oscillations when the link is perturbed. Preliminary results are presented to show that the unit and the proposed control scheme are capable of replicating simulated relative damping values with good fidelity.**

I. Introduction

THE conventional robotic joint implementation found in the majority of robots developed in the past exhibits stiff dynamics as a result of the actuation approach employed which make use of stiff structures actuated by electric brushless or DC motors coupled with high transmission ratio gears and controlled with high gain controllers. These robots work within well defined areas in order to avoid any interaction with the humans, which can be extremely dangerous given their limited safety performance. However, as the areas for technical exploitation have been increased, new demands are placed on the available robotic systems and it has become increasingly clear that the traditionally used stiff robotic systems have significant performance limitations related to safety, efficiency and ability to interact with the environment. In order to address the latest, several compliant actuation robotic prototypes [1-5] have been recently introduced. Although the superior performance of these prototypes systems with respect to safety and efficiency have been successfully demonstrated [2][5], the introduced compliance in the joint drive train forms a limiting factor to the tracking performance that can be achieved by the control system. The compliance embedded in these actuators introduces dynamics which can induce oscillations with a frequency that depend on the stiffness of the joint and the inertia of the link. This complicates the dynamics of the system, especially if a multiple DOF system is considered resulting in a system which is difficult to control.

To regulate the induced oscillations usually the response of the system has to be slowed down. To avoid undesirable oscillations, [6] proposed to pre-shape the position reference by limiting its bandwidth in order to avoid the stimulation of the dynamics of the system. This solution bounds the performance of the system; furthermore the oscillations are not suppressed in the case of interaction with the human and/or environment.

Another solution can be the introduction of damping to suppress the oscillations caused by the compliance of the joint. This damping can be provided by passive, active or semi-active solutions. Passive dampers provide a certain fixed amount of damping. Although this solution is simple, from the robotic application perspective may not be the appropriate since variations on the robotic system configuration and/or the trajectory and loads may require different damping levels. Furthermore, the damping system cannot be disconnected in this case. This is a negative feature as it will reduce the amount of elastic potential energy stored or released in/from the compliant joint. Damping can also be achieved actively by means of impedance/admittance control, [7]. This solution is valid within the closed loop bandwidth of the servo system, which may not be high enough to compensate the high frequency oscillation caused by e.g. a lightweight link and/or a stiff joint.

In contrary to the previous solutions, a semi active damper could facilitate the regulation of the exhibited oscillations without deteriorating the system performance. Looking at the relevant literature several semi-active damping units have been proposed mainly for other applications than robotics, using either friction dampers [8], or magnetorheologial fluids [9], [10].

Matteo Laffranchi is with the Italian institute of Technology (IIT), Genova 16163, Italy and within the University of Sheffield, S10 2TN, UK (e-mail: Matteo.Laffranchi@ iit.it).

N.G.Tsagarakis is with the Italian institute of Technology (IIT), Genova 16163, Italy (phone: +39 010 71781 428; e-mail: nikos.tsagarakis@ iit.it).

D.G.Caldwell is with the Italian institute of Technology (IIT), Genova 16163, Italy (e-mail: darwin.caldwell@ iit.it).

Semi-active adjustable dampers based on magneto-rheological fluids as those developed in [10], [11] can provide variable damping levels on demand. Unfortunately, these solutions are usually cumbersome to fit in a multi-degree of freedom robotic system, e.g. a manipulator. In addition the introduction of liquids within the joint's structure complicates the mechanical design.

In the solution proposed in this work, piezoelectric actuation is used instead to realize a variable damping unit which can provide desired damping levels or be disconnected when required. Moreover, it can make the joint rigid to rotation and therefore effectively managing the potential energy storage and release in the compliant element of the joint. Compared to MR fluids, piezoelectric actuators are clean and lightweight actuators which can be embedded in a compliant joint actuator requiring small additional volume. Semi-active piezoelectric-based friction dampers similar to the prototype presented in this work have been designed for the linear case in [10, 12]. The actuation units used in these works make use of mechanical gearing to gain longer stroke from the piezo actuators. This approach facilitates the mechanical design by raising the range of displacement of the actuator from the microns to the millimeters scale but, on the other hand, the large size of the resulting actuation unit does not match with the demands of compactness required by small scale designs such as the SEA of [4].

This paper presents the realization and control of a new piezoelectric-actuated semi-active variable damping mechanism which can be integrated with a compliant actuator to assist in the damping of the induced oscillations due the joint elasticity. A prototype unit was built to test the feasibility of integration into a compliant actuator.

The paper is structured as follows: Section II introduces the design of the mechanism, Section III presents the model of the semi-active damper while its control is explained in Section IV. Section V presents experimental results from the trials performed in the prototype unit and section VI addresses the conclusions.

II. THE MECHATRONICS OF THE VARIABLE DAMPER

A conceptual schematic diagram of the mechanism introduced in this work is presented in Fig. 1. It consists of the variable damping module and a passive torsion spring element coupled in parallel to the damper in order to induce suitable oscillations as required for the evaluation of the damper performance. A link is fixed at the output of the damper/spring network allowing the installation of different masses which will permit the control of the oscillation frequency.

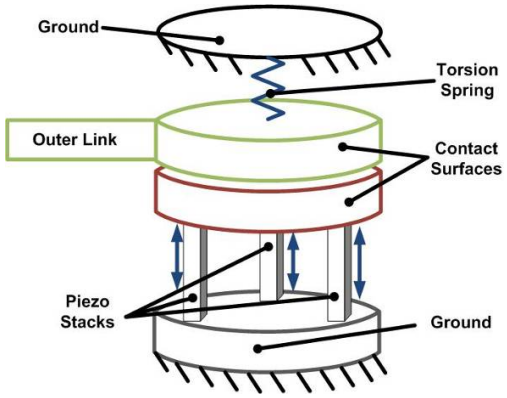

Fig.1 Concept scheme of the mechanism

As shown in Fig.1 three piezo stack actuators connected in parallel are used to apply a force on one of the contact surfaces (brown cylindrical part) which is working against the surface of the green part. The actuators used are three Noliac SCMAP04 piezoelectric stacks with spherical endcaps in order to prevent undesirable bending moments. The actuator's dimensions are 43x5x5 mm, while its weight is 9 g. This prototype was developed to validate the concept; the final objective of this work is to incorporate the damper in the active series elastic actuator presented in [4].

A detailed section of the CAD assembly of the mechanism is depicted in Fig. 2a. The piezo actuators act on the grey part. This intermediate surface behaves as an isolator between the piezo actuators and the first contact surface (brown part), preventing shear forces generated during the link rotation to be applied to the piezo stacks. This is achieved by constraining the relative rotation between the grey and the brown disc by mean of a mechanical constrain. The force generated by the actuators is measured by a ring-shaped load cell which is placed in series between the actuators and the bottom contact surface (brown part).

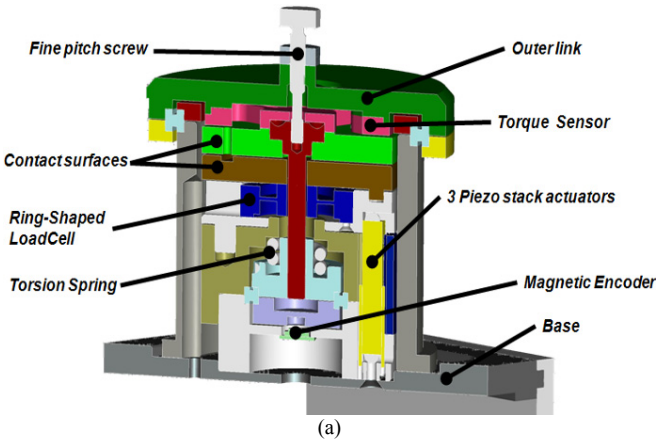

(a)

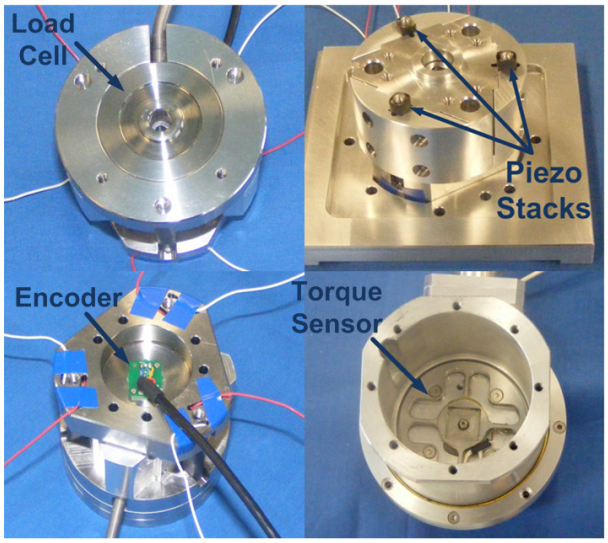

(b)

Fig. 2 (a) Cross section view of the prototype assembly, (b) VPDA's subassemblies

Both the grey and brown components are free to slide along the rotation axis of the link but are rotationally constrained. The top contact surface (light green part) is rigidly connected to the central purple key which provides the connection between the output link and the torsion spring. A prismatic joint between the central key and the output torque sensor allows the displacement of the top contact surface along the rotational axis. This allows the regulation of the distance between the bottom contact and the top contact surfaces. Given the short actuator stroke (Δ_{piezo}=54.7 μm), a fine pitch screw is used for a precise adjustment of this distance in order to bring the two surfaces in proximity to generate the contact within the range of displacement of the piezo actuator. The screw is right-hand threaded on the link side, while a left-hand thread is machined on the red key side, Fig. 2a.

The torque sensor used is a custom made strain gage-based torque sensor which allows the measurement of the torque applied on the unit. The 4-point contact bearing on which the link is mounted makes the torque sensor to be free of forces and thrust moments allowing the measurement of the torque generated around the rotation axis. The position of the link is measured by an AMS AS5045 12 bit absolute magnetic encoder from Austria Microsystems. Deflections larger than the maximum permitted by the spring (±18°) are not allowed by means of mechanical pin based locks.

III. The Dynamics of the Mechanism

This section introduces the mathematical model and system identification of the Variable Physical Damping Actuator (VPDA) prototype.

A. The model of the mechanism

The overall mechanism introduced in the previous section can be modeled as a mass-spring system with friction. For this particular case, it is considered that the magnitude of the friction torque is function of the force generated by the piezoelectric actuators:

$$T_{fric} = \mu_s \cdot F_{piezo}, \dot{\theta} = 0 \quad (1)$$
$$T_{fric} = \mu_d \cdot F_{piezo}, \dot{\theta} \neq 0$$

Where μ_s and μ_d are the equivalent static and dynamic coefficients that take into account the friction coefficient (lubricated steel on steel in this case) and the geometry of the contact surfaces, while F_{piezo} is the force generated by the three piezo actuators. The contact surfaces were lubricated to eliminate the discontinuous effect of the stiction: for this case, the torque can be modeled as in (2)

$$T_{fric} = \mu_d \cdot F_{piezo}, \forall \dot{\theta} \quad (2)$$

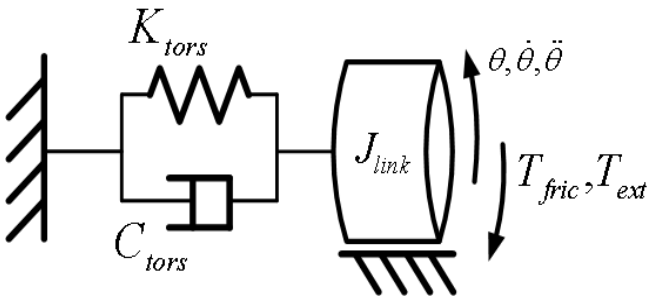

Fig. 3 Model of the semi-active variable damping prototype

The dynamic equation for the model of Fig. 3 is:

$$J_{link} \cdot \ddot{\theta} + C_{tors} \cdot \dot{\theta} + K_{tors} \cdot \theta + T_{ext} + T_{fric} \cdot \mathrm{sgn}(\dot{\theta}) = 0 \quad (3)$$

Where J_{link} is the moment of inertia of the link; C_{tors} is the viscous damping of the assembly; K_{tors} is the stiffness of the torsion spring, T_{fric} is the friction torque generated by the contact surfaces and T_{ext} is the external torque applied. Equation (3) requires the knowledge of the friction coefficient μ_d to fully describe the system. The dynamic friction coefficient was experimentally identified using the prototype system. In these experiments the torsional spring component was temporary removed to allow the free motion of the output link. A number of different normal force levels were manually applied between the two cylindrical contact surfaces. To provide a less noisy normal force for the purpose of the identification the fine pitch screw was used to regulate the normal force instead of the piezo stacks. The level of the normal force was measured by the circular load cell. With the normal applied a slowly raising torque was manually applied to the output link. The applied torque was monitored by the torque sensor while the joint displacement was recorded by means of the absolute encoder. Figure 4 introduces the torsional friction profiles generated by two normal force levels of 90N (a) and 60N (b). Many clockwise-counterclockwise motion cycles have been recorded in this experiment in order to show the variability of torque generated between the cycles. This is

caused mainly by the roughness or the small misalignments between the two surfaces.

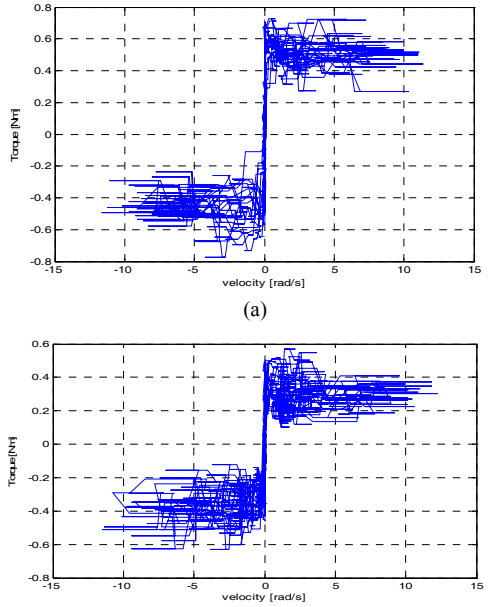

Fig.4 friction torque as a function of the link velocity for a normal force of 90N (a) and 60N (b)

The phenomenon has been modeled as a Coulomb friction without stiction. Mean dynamic friction coefficient values had been retrieved for different normal forces and used to compute a least square fit to retrieve the force-torque line. The resulting line is shown in Fig. 5.

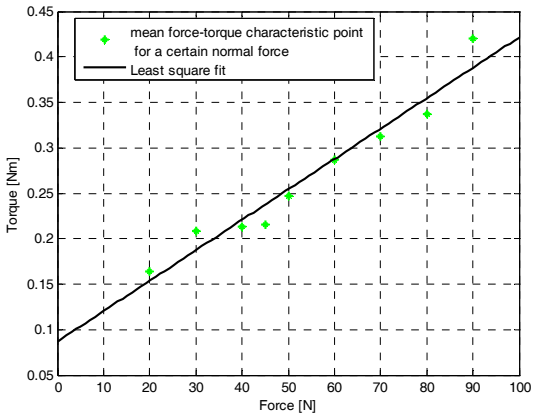

Fig. 5 Force-Torque characteristic

From these measurements the dynamic coefficient of torsional friction were identified to be equal to $\mu_d = 3.3 \cdot 10^{-3}$. The viscous damping coefficient of the system C_{tors} is also needed by (3) and was experimentally retrieved by recording the free response of the system to initial condition. The initial state vector had an initial position of 0.35 rad with respect to the equilibrium position of the spring and a velocity that was equal to zero. The damping ratio was obtained by computing the logarithmic decrement. The obtained viscous damping coefficient was identified to be $C_{tors} = 0.12 Nms \cdot rad^{-1}$. To validate the measurement, the recorded response had been plotted together with the theoretical model, Fig. 6.

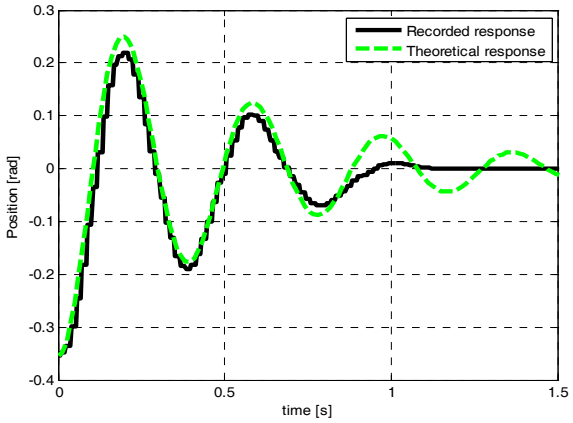

Fig. 6 Initial condition response of the mechanism and model with identified parameters

The resemblance of the two responses is clear until the time t≈0.8sec. After this instant the coulomb friction torque of the assembly, which is generated mainly by the ball bearings and has not been considered in the theoretical model, contrasts the inertial forces making the link to stop in the proximity of the equilibrium position of the spring. The estimated parameters of the system are reported in Tab. 1

TABLE 1
ESTIMATED PARAMETERS OF THE SYSTEM

Parameter	Value
Moment of inertia J_{link}	0.0342 kg·m^2
Stiffness K_{tors}	9.11 Nm·rad^{-1}
Viscous Damping C_{tors}	0.12 Nms·rad^{-1}
Damping ratio ζ	0.11
Friction coefficient μ	3.3·10^{-3} m

IV. SYSTEM CONTROL

The purpose of the system control is to shape the system output response to follow specific desired dynamics. In other words, we would like to make the mass-spring-damper system of Fig. 2 behave like an equivalent mass-spring-adjustable damper system by appropriate control of the force applied by the piezo stacks. Let consider the following equivalent mass-spring damper system with a desired damping C_{des} and inertial and stiffness properties identical to those of the system in Fig. 2.

$$J_{link} \cdot \ddot{\theta} + C_{des} \cdot \dot{\theta} + K_{tors} \cdot \theta = 0 \qquad (4)$$

The desired viscous damping C_{des} as a function of the desired damping ratio ζ_{des} of the equivalent second order system is given by:

$$C_{des} = 2 \cdot \zeta_{des} \cdot \sqrt{K_{tors} \cdot \mathrm{J}_{link}} \qquad (5)$$

By equalizing (4) with (3), for the positive velocity case, without external load applied:

$$C_{des} \cdot \dot{\theta} = C_{tors} \cdot \dot{\theta} + T_{fric} \tag{6}$$

From (6), the friction torque to be generated by the contact surfaces, T_{fric} is obtained:

$$T_{fric} = \left(C_{des} - C_{tors}\right) \cdot \dot{\theta} \tag{7}$$

Introducing in (7) the desired damping ratio as in (5) the T_{fric} can be expressed as a function of the desired damping ratio ζ_{des} of the equivalent second order system

$$T_{fric} = \left(2 \cdot \zeta_{des} \cdot \sqrt{K_{tors} \cdot \mathrm{J}_{link}} - C_{tors}\right) \cdot \dot{\theta} \tag{8}$$

From (8) and (2), the normal force to be generated by the piezo actuators can be obtained:

$$F_{des} = \frac{\left(2 \cdot \zeta_{des} \cdot \sqrt{K_{tors} \cdot \mathrm{J}_{link}} - C_{tors}\right) \cdot \dot{\theta}}{\mu_d} \tag{9}$$

It is important to notice that, although the friction is dependent on the sign of the velocity the solution given by (9) for the positive velocity case gives a positive force also for negative velocities. The force to be generated by the piezoelectric actuators is thus:

$$F_{des} = \frac{\left(2 \cdot \zeta_{des} \cdot \sqrt{K_{tors} \cdot \mathrm{J}_{link}} - C_{tors}\right) |\dot{\theta}|}{\mu_d} \tag{10}$$

This result is explained by the fact that the friction force is always acting in the same direction of the force generated by the viscous damping. This computed force is used as an input for a force loop which is closed on the piezo actuators. The reference force of (10) is affected by the measurement errors of the velocity state and of the estimation of the parameters of the system. In order to compensate for these errors, an outer damping ratio loop had been implemented. In order to feedback the damping ratio it is necessary to estimate this parameter from the measurable states of the system. For a mass-spring-damper system, the viscous damping coefficient can be retrieved from the state-space equation that describes the equilibrium of the torques:

$$C_{meas} = \frac{T_{ext} - \mathrm{J}_{link} \cdot \ddot{\theta} - K_{tors} \cdot \theta}{\dot{\theta}} \tag{11}$$

Where T_{ext} is the external torque applied on the link, J_{link} is the moment of inertia of the link, K_{tors} is the stiffness of the joint, $\theta, \dot{\theta}, \ddot{\theta}$ are, respectively, the angular position, velocity and acceleration of the joint. The difference of the first two terms at the numerator are given by the measurement of the torque sensor, whereas the angular position is measured by the encoder and the angular velocity is obtained through numerical differentiation. The measured viscous damping coefficient as a function of the measurements is therefore:

$$\begin{aligned} C_{meas} &= \frac{T_{meas} - K_{tors} \cdot \theta}{\dot{\theta}}, \dot{\theta} \neq 0 \\ C_{meas} &= C_{des}, \dot{\theta} = 0 \end{aligned} \tag{12}$$

However, when the link is at rest, i.e. $\dot{\theta} = 0$, the damping measurement would return infinite. In order to avoid undesirable behaviour of the system, C_{meas}, ζ_{meas} are set equal to C_{des}, ζ_{des}, respectively, when this condition is verified. According to (5) the damping ratio can be related to the above viscous damping with the following expression

$$\begin{aligned} \zeta_{meas} &= \frac{T_{meas} - K_{tors} \cdot \theta}{2 \cdot \dot{\theta} \cdot \sqrt{K_{tors} \cdot J_{link}}}, \dot{\theta} \neq 0 \\ \zeta_{meas} &= \zeta_{des}, \dot{\theta} = 0 \end{aligned} \tag{13}$$

This provides the measurement of the damping ratio and has been implemented in the "Damping Ratio Estimator" of Fig. 7. Both the force and the damping control loops use standard PID controllers, Fig. 7.

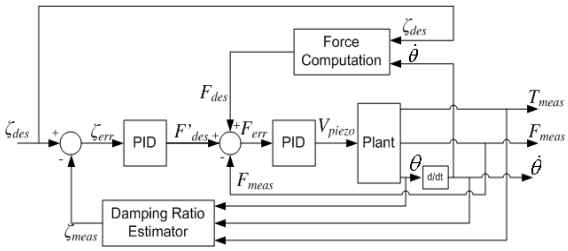

Fig. 7 Control scheme of the unit

Where the block "Force computation" implements (10).

V. Experimental Evaluation

Experiments were carried out in order to test the performances of the unit. The setup used for the tests is shown in Fig. 8.

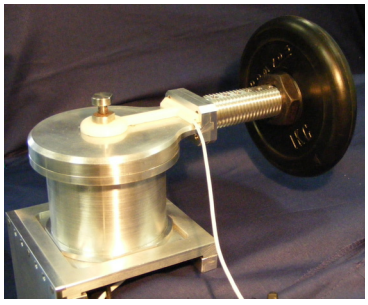

Fig. 8 VPDA prototype unit

Two different tests have been carried out. In a first experiment the spring was removed to evaluate the capability of the variable damper to replicate different damping levels. In a second experiment, trials have been carried out on the full system with the spring inserted.

A. Damping regulation experiment

In this experiment the link of the controlled mass-damper system had been externally perturbed generating different velocities. In this case the viscous damping coefficient was controlled instead of the damping ratio since the second does not have a meaning for this system setup with the spring element removed. The desired damping has been varied progressively from 0.4 to 10 Nms·rad^{-1}. The plot in Fig. 9 shows the torque-velocity characteristic of the system for the simulated viscous damping values of 0.8 and 4 Nms·rad^{-1}. Many clockwise/counterclockwise stimuli cycles are plotted in the graphs.

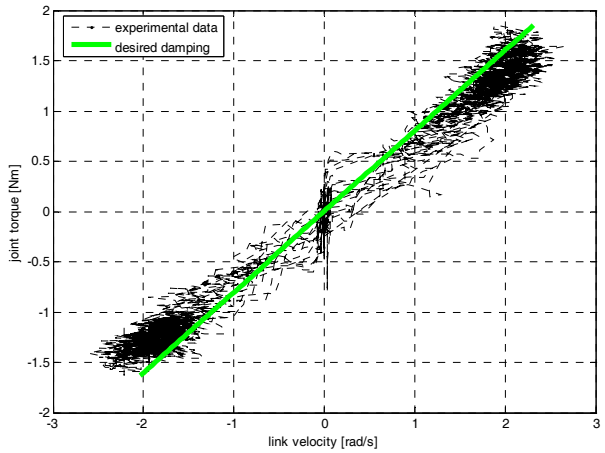

(a)

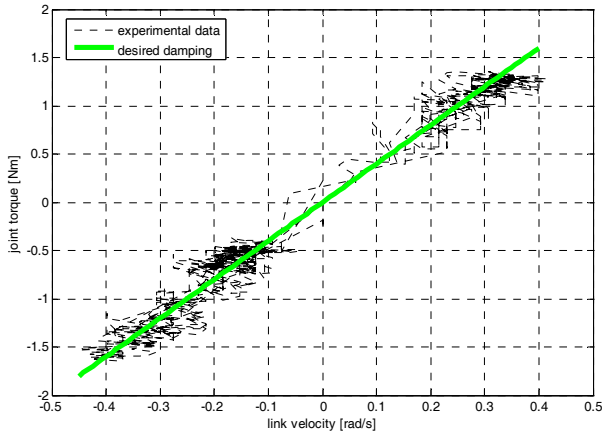

(b)

Fig 9 Torque-Velocity characteristic of a simulated damping of (a) 0.8 Nms/rad and (b) 4 Nms/rad

The plots show that the mean trend of the curve is linear with a slope (Viscous damping coefficient) which is close to the desired viscous damping coefficient.

B. Mass-spring-damper experiment

In this experiment the full Mass-Spring-Damper system was evaluated. The purpose of this test was to damp the free oscillations generated by the Mass-Spring components by applying desired damping ratio. These oscillations were induced by positioning the link at an initial angle outside the equilibrium position of the spring and then releasing it. Different desired damping ratio values progressively increasing from 0.2 to 0.7 were applied.

The plot of the response of the system versus time for the different damping ratios is depicted in Fig. 10.

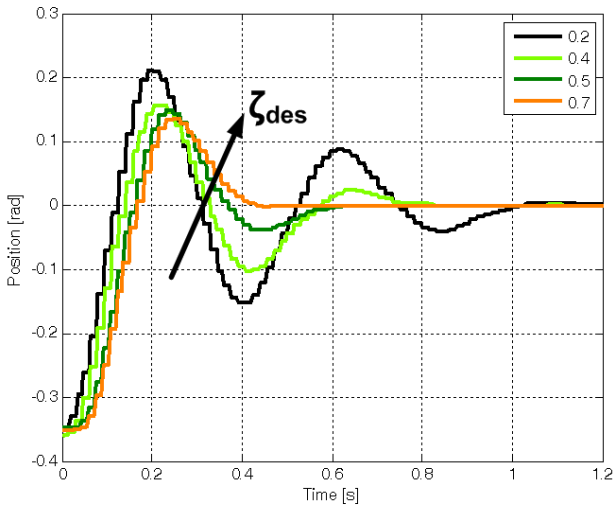

Fig. 10 Time response of the position versus time for different desired damping ratios

Fig. 10 demonstrates the ability of the the semi-active variable damper and its control scheme to successfully replicate the reference damping ratio levels.

VI. CONCLUSIONS AND FUTURE WORK

In this work the design of a new Variable Physical Damping Actuator (VPDA) prototype was presented. The proposed variable damper can form an effective mean for the damping of the oscillations which may occur in a compliant joint. The VPDA presented in this work is a semi-active friction damper which is actuated through piezoelectric actuators. The model and the control scheme of the prototype were analysed. The proposed control scheme is a damping ratio based controller that generates force commands, i.e. the input of a force controller, as a function of the desired damping. The overall system was evaluated with experimental trials performed using a prototype unit.

The preliminary results obtained from these experiments show that the unit and the proposed control scheme are capable of replicating different damping ratios with good fidelity.

Further work will be done on the characterization of the accuracy of the damping tracking. Additional studies will include the comparison of the presented variable physical damping actuator with a system that implements the same

principle without using inner force loop. This will allow the elimination of the force sensor which will permit the more compact integration of the unit.

ACKNOWLEDGMENT

This work is supported by the VIACTORS European Commission FP7-ICT-2007-3 project.

REFERENCES

[1] G. A. Pratt, and M. M. Williamson, "Series elastic actuators," in Intelligent Robots and Systems 95. 'Human Robot Interaction and Cooperative Robots', Proceedings. 1995 IEEE/RSJ International Conference on, 1995, pp. 399-406 vol.1.

[2] M. Zinn, O. Khatib, and B. Roth, "A new actuation approach for human friendly robot design," in Robotics and Automation, 2004. Proceedings. ICRA '04. 2004 IEEE International Conference on, 2004, pp. 249-254 Vol.1.

[3] G. Tonietti, R. Schiavi, and A. Bicchi, "Design and Control of a Variable Stiffness Actuator for Safe and Fast Physical Human/Robot Interaction," in International conference on robotics and automation, Barcelona, Spain, 2005.

[4] N. G. Tsagarakis, Laffranchi, M., Vanderborght, B., Caldwell, D.G., "A Compact Soft Actuator for Small Scale Robotic Systems," in International Conference on Robotics and Automation, Kobe, Japan, 2009.

[5] S. Wolf, and G. Hirzinger, "A new variable stiffness design: Matching requirements of the next robot generation," in Robotics and Automation, 2008. ICRA 2008. IEEE International Conference on, 2008, pp. 1741-1746.

[6] A. L. Edsinger, "Robot Manipulation in Human Environments, PhD Thesis," Massachussets Institute of Technology, 2007.

[7] K. Hirai, M. Hirose, Y. Haikawa *et al.*, "The development of Honda humanoid robot," in IEEE International Conference on Robotics and Automation, 1998, pp. 1321-1326 vol.2.

[8] E. Guglielmino, and K. A. Edge, "Modelling of an electrohydraulically-activated friction damper in a vehicle application," in ASME International Mechanical Engineering Congress & Exposition New York, USA, 2001.

[9] E. Guglielmino, C. W. Stammers, K. A. Edge *et al.*, "Damp-by-wire: magnetorheological vs. friction dampers," in International Federation of Automatic Control (IFAC) 16th World Congress, Prague, Czech Republic, 2005.

[10] M. Unsal, C. Niezrecki, and C. Crane, "Two semi-active approaches for vibration isolation: piezoelectric friction damper and magnetorheological damper," in IEEE International conference on Mechatronics, 2004.

[11] C. Chee-Meng, H. Geok-Soon, and Z. Wei, "Series damper actuator: a novel force/torque control actuator," in Humanoid Robots, 2004 4th IEEE/RAS International Conference on, 2004, pp. 533-546 Vol. 2.

[12] M. Unsal, C. Niezrecki, and C. Crane, "A new semi-active piezoelectric-based friction damper," in Damping and Isolation Conference, San Diego, CA, 2003.